



# The NASA Ames PAH IR Spectroscopic Database: Computational Version 4.00, Software Tools, Website, and Documentation

A. Ricca<sup>1,2</sup> , C. Boersma<sup>1</sup> , A. Maragkoudakis<sup>1,3</sup> , J. E. Roser<sup>1,2</sup> , Matthew J. Shannon<sup>1,4</sup> , L. J. Allamandola<sup>1</sup> , and Charles W. Bauschlicher, Jr.<sup>5</sup>

<sup>1</sup> NASA Ames Research Center, MS 245-6, Moffett Field, CA 94035-1000, USA; [Alessandra.Ricca-1@nasa.gov](mailto:Alessandra.Ricca-1@nasa.gov)

<sup>2</sup> Carl Sagan Center, SETI Institute, 339 Bernardo Avenue, Suite 200, Mountain View, CA 94043, USA

<sup>3</sup> Bay Area Environmental Research Institute, NASA Ames Research Park Building 18, Moffett Field, CA 94035, USA

<sup>4</sup> Universities Space Research Association, Columbia, MD, USA

<sup>5</sup> NASA Ames Research Center, MS 230-3, Moffett Field, CA 94035-0001, USA

Received 2025 August 25; revised 2025 October 29; accepted 2025 October 30; published 2025 December 18

## Abstract

Version 4.00 of the library of computed spectra of the NASA Ames PAH IR Spectroscopic Database (PAHdb) includes an expanded set of polycyclic aromatic hydrocarbon (PAH) spectra, totaling 10,749, calculated using the harmonic approximation and a basis set containing polarization functions. The software tools offered through PAHdb have also been significantly expanded, including optimizations to more efficiently handle the large number of spectra now available. Major improvements have been made to the PAHdb website, which now also offers new libraries of laboratory and computed PAH cluster spectra. PAH boundary-edge codes are now being used throughout PAHdb to hold structural information and to search for specific PAH isomers. All enhancements and updates are described in expanded documentation. As a demonstration, the updated version 4.00 computational library and improved software tools are used to analyze the James Webb Space Telescope spectrum of the atomic photodissociation region of the Orion Bar and show a remarkable improvement in matching the 6.2  $\mu\text{m}$  emission band and the 10–15  $\mu\text{m}$  emission over earlier library versions.

*Unified Astronomy Thesaurus concepts:* [Astronomy databases \(83\)](#)

## 1. Introduction

The NASA Ames PAH IR Spectroscopic Database (PAHdb; C. W. Bauschlicher et al. 2010, 2018; C. Boersma et al. 2014a; A. L. Mattioda et al. 2020) contains the data, models, software, and website<sup>6</sup> created to support the detailed investigation of the infrared (IR) emission features seen throughout the interstellar medium (ISM), which have been attributed to polycyclic aromatic hydrocarbon (PAH) molecules (A. G. G. M. Tielens 2008).

PAHdb offers libraries of density functional theory (DFT), 0 K, computed spectra for a large variety of PAH molecules, libraries of laboratory measured PAH and PAH-related spectra, software to work with data when downloaded, a web portal, and extensive documentation. PAHdb has been used to study a wide range of astronomical objects and environments, including the ISM (e.g., C. Boersma et al. 2018; M. J. Shannon & C. Boersma 2019; R. X. Zang et al. 2019; A. Sidhu et al. 2022), the Galactic center (e.g., L. S. Bernstein & T. R. Geballe 2024), galaxies (e.g., A. Maragkoudakis et al. 2022), and starbursts (e.g., Y. Martins-Franco & K. Menéndez-Delmestre 2021). PAHdb also has planetary and terrestrial applications, such as investigating haze-forming planetary atmospheres (M. López-Puertas et al. 2013; B. P. Coy et al. 2023) or investigating the soil chemistry of Earth and Mars (N. Kopacz et al. 2023).

PAHdb has also contributed to a number of ISM investigations including determinations of the principal PAH emission components established through blind signal separation (M. J. F. Rosenberg et al. 2011) or machine learning (P. Kovács et al. 2020) techniques, assessment of the universality of the astronomical PAH spectrum (M. J. F. Rosenberg et al. 2014), an in-depth investigation into the origin of the 12.7  $\mu\text{m}$  PAH emission band (A. Candian et al. 2014), a determination of the size distribution of interstellar PAHs (B. A. Croiset et al. 2016), and a study of the catalytic formation of molecular hydrogen on interstellar PAHs (H. Andrews et al. 2016). PAHdb has been used to evaluate the “GrandPAH” hypothesis that local variations in the ISM PAH emission bands are due to variations in the PAH populations that can survive within the corresponding local ISM radiation environments (H. Andrews et al. 2015). PAHdb has also been used to develop calibration charts to directly translate PAH band strength ratios into diagnostic characteristics of the PAH population (A. Maragkoudakis et al. 2020, 2023a, 2023b).

The inaugural version of PAHdb, containing a large collection of theoretically computed and laboratory measured IR spectra of PAHs at 0 K, was made publicly available in 2010 (C. W. Bauschlicher et al. 2010). The library of computed PAH spectra featured 583 DFT spectra. In 2013, version 2.00 of the library of computed spectra was released (C. Boersma et al. 2014a), expanding it to a total of 700 spectra that featured larger PAHs. Version 3.00, released in 2018, introduced the use of multiple scale factors to align the theoretical harmonic frequencies with the experimental fundamentals instead of the single scaling factor used previously (C. W. Bauschlicher et al. 2018). The library of laboratory measured spectra was updated to version 3.10 in 2020 to

<sup>6</sup> <https://www.astrochemistry.org/pahdb/>



Original content from this work may be used under the terms of the [Creative Commons Attribution 4.0 licence](#). Any further distribution of this work must maintain attribution to the author(s) and the title of the work, journal citation and DOI.

include 84 species (A. L. Mattioda et al. 2020). Finally, version 3.20 of the computed library added multiple new spectra of totally resonant sextet (also denoted “Clar PAHs”) to PAHdb, as well as numerous spectra of PAHs containing only straight edges (see Section 2.2 for a detailed comparison of spectra available in v4.00 compared to spectra available in version 3.20).

Ongoing analysis of the increasingly expansive and detailed catalog of observations of interstellar PAH emission including observations provided by the ongoing James Webb Space Telescope (JWST) mission (R. Chown et al. 2024; S. Pasquini et al. 2024) continues to prompt expanding the contents of PAHdb’s spectral libraries, adding new spectral libraries of PAH-related species, improving and expanding the offered models, and further developing the software tools.

This paper reports on version 4.00 of a library of computed PAH spectra that adds over 6500 spectra, a newly added library of computed PAH cluster spectra (version 1.00), and the associated library of laboratory measured PAH cluster spectra (version 1.10), along with updates made to the software tools, website improvements, and expanded documentation.

This paper is organized as follows: Section 2 describes the newly added content, and Section 3 describes the updated software tools. Section 4 describes additions and improvements to the PAHdb website, and Section 5 describes the expanded PAHdb user documentation. Section 6 applies PAHdb version 4.00 improvements to the analysis of a JWST spectrum of the Orion Bar. Finally, the paper finishes with a summary of improvements and future plans for PAHdb in Section 7.

## 2. Content

### 2.1. Computational Method

Geometry optimizations and harmonic calculations were performed using DFT, the harmonic approximation, the B3LYP hybrid functional (A. D. Becke 1993; P. J. Stephens et al. 1994), and the Gaussian 09 (M. J. Frisch et al. 2009) and Gaussian 16 (M. J. Frisch et al. 2016) suites of programs. For version 3.20, spectra were computed using the 4–31G basis set (M. J. Frisch et al. 1984) and the harmonic frequencies were scaled using a single scale factor of 0.958, which has been shown to bring the computed spectra in good agreement with matrix-isolation experiments (C. W. Bauschlicher & A. Ricca 2010). For version 4.00, all spectra were computed using the larger basis set 6–31G\* (M. J. Frisch et al. 1984), which includes polarization functions that allow a better description of the redistribution of charge occurring during the vibrations. The harmonic frequencies were scaled using three scaling factors, namely, 0.964 for C–H stretches around  $3\ \mu\text{m}$ , 0.979 for bands between 4 and  $9\ \mu\text{m}$ , and 0.975 for bands beyond  $9\ \mu\text{m}$ . These scale factors were obtained by fitting the theoretical data to 25 bands obtained from gas-phase PAH laboratory experiments, which included 17 IR allowed bands and one  $A_u$ , one  $B_{1g}$ , two  $B_{2g}$ , and four  $A_g$  bands (F. M. Behlen & S. A. Rice 1981; E. Cané et al. 1996; O. Pirali et al. 2009). The cluster calculations were carried out using the B3LYP functional and the dispersion term of Grimme (S. Grimme 2006) to account for the van der Waals interactions between the PAH monomers, the 4–31G basis set (M. J. Frisch et al. 1984), and the Gaussian 09

suite of programs (M. J. Frisch et al. 2009). The harmonic frequencies were scaled using a single scale factor of 0.958.

### 2.2. Library of PAH Spectra

A detailed description of the new PAHs added to version 4.00 is provided in Table 1. Version 4.00 has a net increase of 6516 spectra compared to version 3.20, which includes 4651 new spectra of pure PAHs (only C and H atoms) with edge defects such as bay regions (A. Ricca et al. 2024) and 1866 new spectra of nitrogenated PAHs (A. Ricca et al. 2021). The dication spectra for all the species in version 3.20 are now included in version 4.00, and 2843 new dication spectra were added. Version 3.20 of the library of computed spectra also provides version 4.00 with the spectra of PAHs with straight edges (A. Ricca et al. 2018) and the spectra of numerous Clar PAHs, which have edge structures dominated by armchair edges (A. Ricca et al. 2019). Figure 1 shows that for pure PAHs, the largest amount of spectra was added for mid-sized PAHs with  $\sim 50$  carbons, and about half of that amount was added for larger PAHs containing  $\sim 70$  and  $\sim 100$  carbons. For small and very large PAHs, fewer spectra were added. For nitrogenated PAHs, the largest amount was for large PAHs containing  $\sim 100$  carbons, which contained up to three nitrogen atoms. Figure 2 shows that a large number of dications were added for  $\sim 50$  carbons, which constituted a large fraction of species in version 3.20. A significant number of doubly and triply charged species were computed for nitrogenated PAHs containing about 100 carbons, given the presence of the nitrogen atoms, which are more electronegative than the carbon atoms. The fraction of neutrals (42%) and cations (47%) is comparable, whereas anions constitute a smaller fraction of 11%; pure PAHs are dominant (81%) with nitrogenated PAHs constituting 19% (see Figure 3).

### 2.3. Libraries of PAH Cluster Spectra

*Computational.* A newly introduced computed library (version 1.00) containing the spectra of 103 clusters has been made available. It holds computed spectra of neutral clusters of pyrene ( $\text{C}_{16}\text{H}_{10}$ ), coronene ( $\text{C}_{24}\text{H}_{12}$ ), ovalene ( $\text{C}_{32}\text{H}_{14}$ ), and 3,4,5,6,7,8-tribenzoperopyrene<sup>7</sup> ( $\text{C}_{34}\text{H}_{16}$ ; A. Ricca et al. 2013). Figure 4 illustrates the cluster conformations, which include single stack (“step” and “graphite” conformations) and multiple stack (“herringbone” or “intertwined” conformations). Investigated cluster structures had up to 10 monomer units.

Pericondensed PAHs assemble by first forming single stacks. The number of monomers per stack depends on PAH size and shape. The number of monomers per stack increases with PAH size, and PAHs with disklike shapes form single stacks with the largest number of monomers.

Pyrene is the smallest PAH with a disklike shape. It forms single stacks containing up to three or four monomers. For five monomers and higher, the single stacks form multistacked conformations that we denote intertwined, which are consistent with X-ray data (G. R. Desiraju & A. Gavezzotti 1989a, 1989b). Coronene is larger than pyrene and also has a disklike shape. It forms single stacks containing up to six monomers and multistacked conformations for seven monomers and up that are in agreement with previous theoretical

<sup>7</sup> For clarity, we use the structure name adopted in the cited works. The IUPAC name for this structure is benzo[*pqr*]dinaphtho[8,1,2-*bcd*:2',1',8'-*lmn*]perylene (L. C. Sander & S. A. Wise 2020).

**Table 1**  
Breakdown of the Molecules Included in Version 4.00 of the Computational Database by Charge, Composition, and Size

Charge	Number of Carbon Atoms							Total
	1–10	11–20	21–30	31–50	51–70	71–100	101–386	
All molecules								
all	88(12)	271(57)	1355(502)	3689(1922)	1558(1056)	3014(2579)	774(388)	10,749(6516)
neutral	39(0)	114(-2)	798(0)	1892(268)	535(374)	901(755)	200(64)	4479(1459)
anion –	3(0)	11(0)	21(7)	193(135)	225(88)	599(474)	179(63)	1231(767)
cation +	34(0)	87(0)	41(7)	351(272)	547(359)	903(744)	199(65)	2162(1447)
++/+++	12(12)	59(59)	495(488)	1253(1247)	251(235)	611(606)	196(196)	2877(2843)
PAHs without substitutions								
all	38(12)	181(57)	1326(498)	3652(1900)	1384(914)	1303(882)	774(388)	8658(4651)
neutral	12(0)	69(-2)	786(-1)	1882(259)	491(332)	470(324)	200(64)	3910(976)
anion –	3(0)	9(0)	18(4)	184(126)	185(48)	172(47)	179(63)	750(288)
cation +	11(0)	44(0)	30(7)	333(268)	492(328)	470(325)	199(65)	1579(993)
++/+++	12(12)	59(59)	492(488)	1253(1247)	215(205)	191(186)	196(196)	2418(2393)
PAHs with nitrogen								
all	10(0)	48(0)	22(4)	31(22)	161(143)	1705(1697)	0(0)	1977(1866)
neutral	5(0)	24(0)	12(1)	9(9)	42(42)	431(431)	0(0)	523(483)
anion –	0(0)	2(0)	3(3)	9(9)	40(40)	427(427)	0(0)	481(479)
cation +	5(0)	22(0)	7(0)	13(4)	43(31)	427(419)	0(0)	517(454)
++/+++	0(0)	0(0)	0(0)	0(0)	36(30)	420(420)	0(0)	456(450)
PAHs with oxygen								
all	40(0)	42(0)	0(0)	0(0)	2(0)	0(0)	0(0)	84(0)
neutral	22(0)	21(0)	0(0)	0(0)	0(0)	0(0)	0(0)	43(0)
anion –	0(0)	0(0)	0(0)	0(0)	0(0)	0(0)	0(0)	0(0)
cation +	18(0)	21(0)	0(0)	0(0)	2(0)	0(0)	0(0)	41(0)
++/+++	0(0)	0(0)	0(0)	0(0)	0(0)	0(0)	0(0)	0(0)
PAHs with magnesium or iron								
all	0(0)	0(0)	7(0)	6(0)	12(0)	6(0)	0(0)	31(0)
neutral	0(0)	0(0)	0(0)	1(0)	2(0)	0(0)	0(0)	3(0)
anion –	0(0)	0(0)	0(0)	0(0)	0(0)	0(0)	0(0)	0(0)
cation +	0(0)	0(0)	4(0)	5(0)	10(0)	6(0)	0(0)	25(0)
++/+++	0(0)	0(0)	3(0)	0(0)	0(0)	0(0)	0(0)	3(0)
PAHs without hydrogen								
all	0(0)	10(0)	295(0)	494(-1)	10(0)	3(0)	0(0)	812(-1)
neutral	0(0)	10(0)	294(0)	494(-1)	4(0)	1(0)	0(0)	803(-1)
anion –	0(0)	0(0)	0(0)	0(0)	2(0)	0(0)	0(0)	2(0)
cation +	0(0)	0(0)	1(0)	0(0)	4(0)	1(0)	0(0)	6(0)
++/+++	0(0)	0(0)	0(0)	0(0)	0(0)	1(0)	0(0)	1(0)

**Note.** The difference in the number of species in each class with version 3.20 is given in parentheses.

results (M. Rapacioli et al. 2005a). Ovalene is larger than coronene and has an oval disklike shape, leading to the formation of single stacks containing up to seven monomers and multistacked arrangements for a larger number of monomers. For these three disklike molecules, the packing follows similar trends, whereas for 3,4;5,6;7,8-tribenzoperopyrene ( $C_{34}H_{16}$ ), which has more eroded edges, the single stacks contain only up to four monomers despite the larger size of the monomer. Clustering induces a redshift of the computed C–H out-of-plane bending ( $CH_{oop}$ ) IR bands between 10 and 15  $\mu m$  that can range from 2 to 8  $cm^{-1}$ , depending on the PAH monomer and a broadening of the bands.

**Laboratory.** A library (version 1.10) of laboratory measured IR spectra that demonstrates the effects of PAH clustering in the C–H stretching ( $\sim 3.3 \mu m$ ) and C–H out-of-plane bending regions

( $\sim 10$ – $15 \mu m$ ) has also been added to PAHdb (J. E. Roser & L. J. Allamandola 2010; J. E. Roser et al. 2014; J. E. Roser & A. Ricca 2015). For each of the eight PAH molecular species investigated, IR transmission measurements were made for a series of PAH/argon ice mixtures, each mixture newly deposited in vacuum onto a 5 K cesium iodide substrate before measurements were recorded. Each deposit used a distinct argon/PAH ratio that varied between high dilution of PAH (ratio  $\sim 1000$  or higher) to very low dilution of PAH (ratio  $\sim 100$  or less). As the dilution decreases, clustering of PAH molecules within the argon matrix increases, and absorption features of PAH clusters become more apparent within the spectra.

In these experiments, the spectra of the compact PAH molecules pyrene and benzo[ghi]perylene exhibited cluster features in the C–H out-of-plane bending region that were

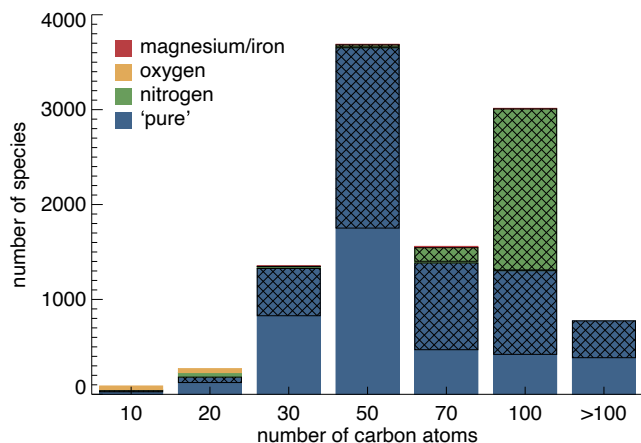


**Figure 1.** Breakdown of the PAHs in version 4.00 of the library of computed spectra by composition and number of carbon atoms. “Pure” PAHs contain only carbon and hydrogen; nitrogen refers to PAHs containing nitrogen as well. The cross-hatched areas indicate the additions between versions 3.20 and 4.00.

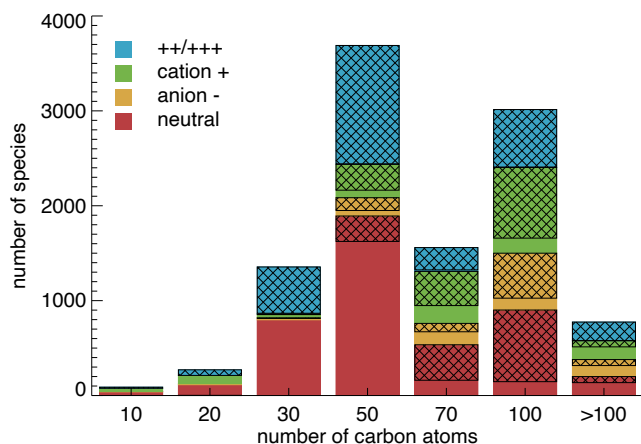


**Figure 2.** Breakdown of the PAHs in the library of computed spectra by charge and number of carbon atoms. The cross-hatched areas indicate the additions between versions 3.20 and 4.00.

redshifted by  $1\text{--}4\text{ cm}^{-1}$  compared to the same features in the dilute matrices (J. E. Roser & A. Ricca 2015). This redshift is similar in magnitude to that determined by theoretical calculations ( $2\text{--}8\text{ cm}^{-1}$ ) and similar in magnitude to a well-known shift of the  $11.20\text{ }\mu\text{m}$  interstellar band to  $\sim 11.25\text{ }\mu\text{m}$  (or  $\sim 3.97\text{ cm}^{-1}$ ).

It has often been proposed that the  $11.25\text{ }\mu\text{m}$  component of the  $11.2\text{ }\mu\text{m}$  band can therefore be attributed to PAH clusters or very small grains (M. Rapacioli et al. 2005b; P. Pilleri et al. 2012; S. Pasquini et al. 2024). Our computed and laboratory data support the hypothesis that clustering of PAHs contributes to the redshifting of the  $11.2\text{ }\mu\text{m}$  band (J. E. Roser & A. Ricca 2015, 2020).

#### 2.4. Boundary-edge Code Description

The website and software functionality described below also make use of the boundary-edge code for polyhexes of P. Hansen et al. (1996). A boundary-edge code is a sequence of digits representing a traversal of the boundary hexagons of a PAH molecule that notes the number of exterior edges per hexagon, so that naphthalene (having two rings with five exterior edges each) would be represented as “55,” chrysene

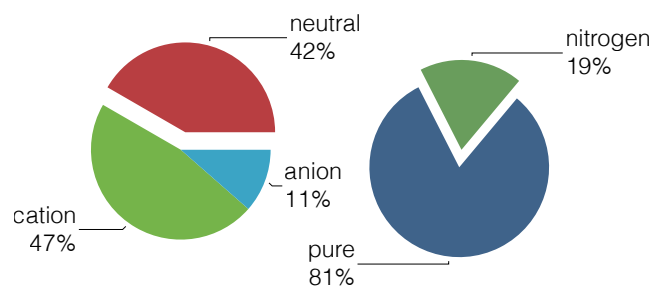


**Figure 3.** Pie charts showing the distribution of PAH charge (left) and composition (right) in version 4.00 of the library of computed spectra in percentages. *Nitrogen* refers to PAHs containing one or more nitrogen atoms, and *pure* refers to PAHs comprised solely of carbon and hydrogen.

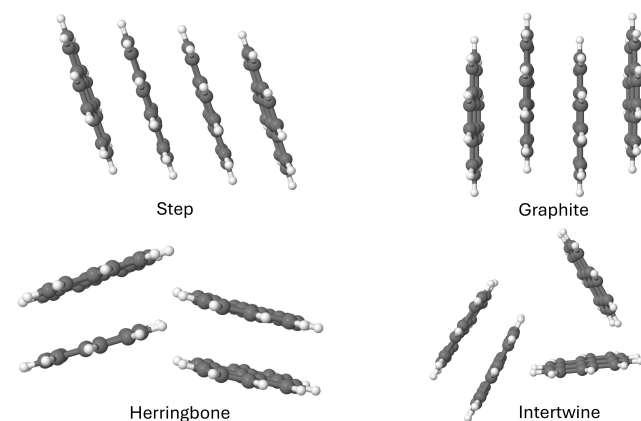


**Figure 4.** The various cluster conformations illustrated using pyrene tetramer.

would be represented as “531531,” etc. For simplicity, we denote digit sequences that differ only by cyclic permutation and/or reversal of the order of digits as also being boundary-edge codes representing the same polyhex instead of reserving the term for only the lexicographically maximal sequence.

A boundary-edge code will uniquely identify a non-helicene PAH (X. Guo et al. 2002) and can be used to readily identify properties of the PAH structure, such as its hydrogen atom and carbon atom counts, its hydrogen atom adjacency classes, the symmetries of the PAH structure, and the number of hexagons in the structure (P. Hansen et al. 1996; J. Kovič 2014). A boundary-edge code, therefore, provides a compact representation of a PAH molecule that is convenient to use in software applications and that provides relatively rapid computation of its structural properties. As illustrated below, these properties of boundary-edge codes make them particularly useful for implementing PAH isomer-specific searches in PAHdb.

### 3. Software

PAHdb offers three software suites that can be used to interact with the database offline and to analyze and interpret astronomical observations. These are the AmesPAHdbIDL-Suite (The PAHdb Team 2025), AmesPAHdbPythonSuite (The PAHdb Team 2022), and pyPAHdb (The PAHdb Team 2024).

The abandonment of the general descriptor  $\text{CH}_x$  to indicate aliphatic side groups and the introduction of CH and  $\text{CH}_3$  for added granularity in version 4.00 of the library of computed spectra necessitated changes to the XML parsing codes used by the software. To retain backward comparability with earlier



library versions, the descriptors CH, CH<sub>2</sub>, CH<sub>3</sub>, and CH<sub>x</sub> remain all valid.

A demonstration of pyPAHdb and the Python suite was given at JWebbinar 23<sup>8</sup> and 42<sup>9</sup> as part of the series of virtual seminars provided by the Space Telescope Science Institute that aimed to the JWST community about tools and methods to analyze data from JWST.

### 3.1. AmesPAHdbIDLSuite

The AmesPAHdbIDLSuite (C. Boersma et al. 2014a) is written in IDL<sup>10</sup> and is the most mature of the software packages. The IDL suite contains the IDL implementation of PAHdb's primary computational task: calculating the IR emission spectrum due to an ensemble of PAH molecules for comparison with observed interstellar spectra. With the increasingly larger library of computed spectra, it has become pertinent for the IDL suite to be more efficient when handling the data. To this end, a number of improvements have been made that allow for speedier data operations.

A first speedup was to replace WHERE calls, which require linear search, with the much faster HISTOGRAM reverse lookup calls. Another speedup is relying heavily on lazy instantiating. For example, when requesting a subclass breakdown (e.g., charge, size, etc.) of a database fit, the breakdown is computed once and then internally cached for fast subsequent retrieval. Applying a PAH emission model can be a particularly time-consuming task. The IDL suite now automatically caches the results of such tasks, so a subsequent request for the same data does not require repeating these computations. The cached data can be saved to disk, so it is persistent across different IDL sessions as well as complete system reboots.

Recognizing when the results of a PAH emission model have been cached is achieved by creating a hash key from the parameters of the emission model and the database used and comparing it to files saved to disk. Finally, the breakdown of a spectroscopic fit now introduces a medium-sized class that defaults to  $50 \leq N_{\text{carbon}} < 90$ . Functionality has been added to the suite to manage the cached data by setting the local cache location, deleting unneeded cached files, etc.

The provided non-negative least-square (NNLS) routine now accepts supplying both a tolerance and maximum number of iterations, which default to  $10^{-16}$  and 128, respectively. One can now provide the NNLS routine with a callback function to monitor progress at each iteration.

Although the IDL suite can take observational uncertainties into account when fitting (NNLC; P. Désesquelles et al. 2009) astronomical data, it previously lacked a mechanism to provide uncertainties for any of its derived parameters. This has now been solved by the implementation of a Monte Carlo approach that refits the spectrum a given number of times upon permuting the input observational spectrum within its associated uncertainties to obtain a distribution for the derived parameters. This method has been, for example, successfully applied by C. Boersma et al. (2024) to study the PAH emission from the (diffuse) background ISM. See also Section 6 and the Appendix.

A full CHANGELOG of the IDL Suite is maintained at <https://github.com/PAHdb/AmesPAHdbIDLSuite/blob/master/CHANGELOG.txt>.

### 3.2. AmesPAHdbPythonSuite

The AmesPAHdbPythonSuite,<sup>11</sup> first announced in A. L. Mattioda et al. (2020), is the Python counterpart to the AmesPAHdbIDLSuite (Section 3.1). It mirrors the IDL application programming interface (API) and also relies upon XML files downloaded from the PAHdb website.

The AmesPAHdbPython suite currently works with libraries of DFT-computed and laboratory measured spectra. To efficiently handle large datasets, the Python suite leverages multiprocessing, where it can be used, e.g., in the application of a PAH emission model.

As of version 0.5.0, the AmesPAHdbPythonSuite includes (i) a comprehensive search interface for finding and selecting PAHs; (ii) interactive 3D-visualization of chemical structures using *vtk*; (iii) retrieval of molecular parameters like number of *n*-rings, area, and weight, and a routine for estimating a boundary-edge code of a PAH structure based upon its list of atom coordinates in PAHdb; (iv) Python versions of all PAH emission models available in the IDL version (*FixedTemperature*, *CalculatedTemperature*, and *Cascade*); (v) the option to use approximations in the PAH emission models per E. L. O. Bakes et al. (2001a, 2001b); (vi) the option to compute the average energy absorbed by a PAH from a stellar blackbody at a given temperature; (vii) the option to compute the average energy absorbed by a PAH from a stellar model such as those by F. Castelli & R. L. Kurucz (2003); (viii) the option to compute the average energy absorbed by a PAH from the interstellar radiation field as described by J. S. Mathis et al. (1983); (ix) convolution of spectral bands with either a Gaussian, Lorentzian, or Drude line profile with a given full width at half-maximum (FWHM); (x) coaddition of PAH spectra; (xi) reading in astronomical data in a number of formats, relying on functionality provided by the *specutils*<sup>12</sup> and *astropy*<sup>13</sup> packages; (xii) fitting astronomical PAH spectra; (xiii) retrieving PAH size, charge, and composition subclass breakdown from fits; (xiv) fitting astronomical PAH spectra using a Monte Carlo approach that provides uncertainty estimates for the subclass breakdowns, and (xv) providing quality of fit measures for both the total fit and on a per PAH band basis.

This Monte Carlo method has been, for example, successfully applied by A. Maragkoudakis et al. (2022) and A. Maragkoudakis et al. (2025b) to study the PAH emission from galaxies. See also Section 6 and the Appendix.

Differences between the IDL and Python suites include the option for a wavelength-dependent FWHM when convolving line profiles (IDL), computing boundary-edge codes (Python), and a cache manager (IDL). Furthermore, due to implementation differences, e.g., the composite trapezoidal rule used for integration in Python and a five-point Newton–Cotes method in IDL, results can vary slightly. Lastly, since it is the most mature of the two, the AmesPAHdbIDLSuite has, thus far, received the most optimizations and, therefore, in some scenarios, there can be a performance advantage.

<sup>8</sup> <https://www.pdrs4all.org/meeting-announcements/>

<sup>9</sup> <https://astrochemistry.org/pahdb/jwebbinar-42>

<sup>10</sup> IDL is registered by NV5: <https://www.nv5geospatialsoftware.com/Products/IDL>.

<sup>11</sup> <https://github.com/PAHdb/AmesPAHdbPythonSuite>

<sup>12</sup> <https://specutils.readthedocs.io/en/stable/index.html>

<sup>13</sup> <https://docs.astropy.org/en/stable/index.html>

### 3.3. pyPAHdb

pyPAHdb<sup>14</sup> is a Python package developed as part of the PDRs4All<sup>15</sup> JWST Early Release Science (ERS) program (ID 1288; O. Berné et al. 2022) and was first described in M. J. Shannon & C. Boersma (2018). Its aim is to quickly and conveniently fit the PAH emission component of a JWST spectrum and identify components due to specific PAH charge states and sizes. The user is responsible for isolating the PAH emission spectrum from any other components in the observations before modeling with PAHdb. pyPAHdb streamlines the database fitting approach when compared to using the Python suite (Section 3.2) by giving up some flexibility. This is achieved by using a *precomputed* matrix of highly oversampled synthesized PAH emission spectra. The matrix is now built from version 3.20 (C. W. Bauschlicher et al. 2018) of the library of computed spectra, and in future releases, it will provide the option to download libraries optimized for the modeling of specific astronomical object types (e.g., galaxies, H II regions, etc.).

pyPAHdb has seen numerous improvements and has been used to analyze both Spitzer (e.g., E. Kosmaczewski et al. 2022) and JWST (e.g., A. Maragkoudakis et al. 2025b) data. Because JWST data can be sizable, pyPAHdb relies heavily on parallelization and has been optimized to handle large spectral mosaics like that of the Orion Bar from the PDRs4All ERS program (A. Maragkoudakis et al. 2025a). Nonetheless, single spectra, provided in a variation of formats, can also be analyzed. Quick-look products like maps and the spectral decomposition of individual pixels are generated and saved to PDF upon request. The final output is stored in the FITS format (W. D. Pence et al. 2010) and includes separate extensions for the charge (cation, neutral, and anion) and size (small, medium, and large) fractions, the cation over neutral ratio, and the fitting uncertainty.

## 4. Website

The data in the database can be downloaded from <https://www.astrochemistry.org/pahdb/> as XML-structured data or with a simple ASCII text structuring. Older versions of the data will also remain available for download. The website interface allows one to interrogate the database and make selections. A number of advanced tools are available that give visitors the ability to work with PAH spectra directly online. The PAHdb website provides an extensive help section to guide users.

Abandonment of the general descriptor  $\text{CH}_x$  and introduction of CH and  $\text{CH}_3$  necessitated changes to the MySQL tables, the XML parsing code, as well as to numerous other parts of the website.

Since the reporting in A. L. Mattioda et al. (2020), the website has seen a number of improvements. For example, it now offers the download of cluster data (see Section 2.3) and provides an intuitive visualization to explore them. PAH monomer species that have associated cluster data will show a red dot above their chemical formula when browsing/searching the database contents. One can also search for species with cluster data directly using the term “clusters.” Cluster data are presented in a dedicated “Clusters” tab on a

species’ “Details” page. For the library of computed PAH cluster spectra, the different available conformations and number of monomers are shown, organized in a matrix. Subsequently, clicking an entry will present a page similar to a PAH species’ “Details” page. In the case of the library of laboratory measured PAH cluster spectra, the “Clusters” tab directly graphs the spectra at different concentrations. Google’s Chartjs library is employed to do the visualization, which is now also used to display the laboratory spectra in the library of laboratory measured PAH spectra and allows for panning, zooming, etc.

Visualization of spectral data has been improved with graphs that show both a wavelength (in microns) and frequency (in wavenumbers) axis. This includes those produced by the C++ backend<sup>16</sup> that drives the online tools. The C++ back-end has been updated to use the C++17 standard, embracing isomorphism, relying on smart pointers, etc. The parts interacting directly with PAHdb’s underlying MySQL database were modified to deal with the changes related to aliphatic side groups (see Section 3).

In addition, the online tools can now apply a PAH emission model to the laboratory data, which was not possible before now. For this, the empirical approximations described by E. L. O. Bakes et al. (2001a) are used. It is noted that the online tools have been applied to analyze and interpret astronomical observations (e.g., A. Silva-Ribeiro et al. 2022). Figure 5 shows the “Results” page when using the “Stack” tool with only coronene ( $\text{C}_{24}\text{H}_{12}$ ) from the library of laboratory measured PAH spectra selected. In this example, a full temperature cascade PAH emission model is applied using an excitation energy of 8 eV, and each transition is convolved with a Drude emission profile with an FWHM of  $15.0\text{ cm}^{-1}$ . The tool is configured to use wavelength for the primary (bottom)  $x$ -axis, which can be set in the General options.

Searches for pure PAH structures can now use a boundary-edge code input to guide the search. This can be a convenient search option since it may be easier for a user to convert a visual representation of a PAH structure into a boundary-edge code than it is for the user to manually enumerate its hydrogen and carbon atom counts. Figure 6 illustrates the convenience that using the boundary-edge code can often provide. In this figure, a PAHdb version 4.00 search for the  $\text{C}_{96}\text{H}_{30}$  PAH structure named “superphenalene” (V. S. Iyer et al. 1997) using its boundary-edge code is able to immediately bring up the relevant structure in the search results. Performing a similar search using carbon atom and hydrogen atom counts only, i.e., using the search string “C = 96, H = 30,” might require a user to manually count carbon atoms and hydrogen atoms of a 34-ring PAH structure and/or sort through 65  $\text{C}_{96}\text{H}_{30}$  search results to find the superphenalene structure.

At present, a database search using a boundary-edge code input is not fully isomer-specific since the input code is used to generate a PAHdb search string containing the number of carbon atoms, hydrogen atoms, and hydrogen adjacency as computed from the input code. A fully isomer-specific search using a boundary-edge code input is a possibility for a future version of PAHdb.

<sup>14</sup> <https://github.com/PAHdb/pyPAHdb>

<sup>15</sup> <https://pdrs4all.org>

<sup>16</sup> <https://github.com/PAHdb/CPP-Backend>

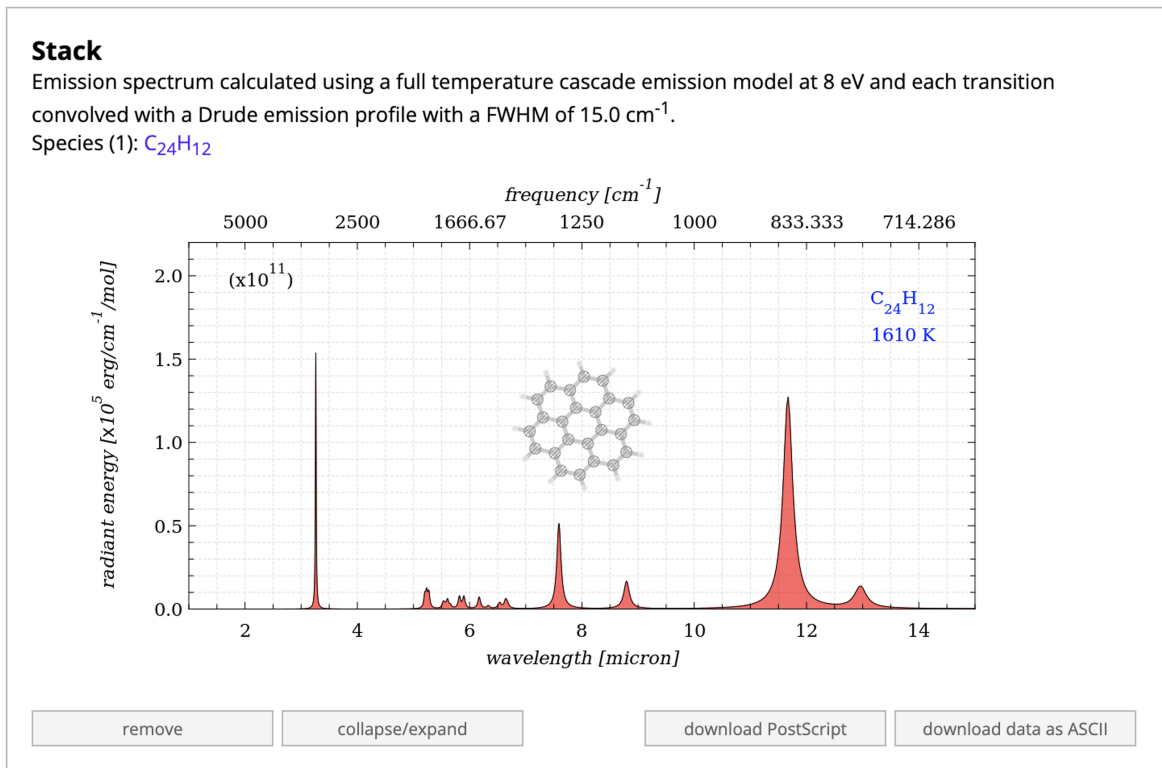


**Figure 5.** Full temperature cascade PAH emission model applied to the laboratory measured spectrum of neutral coronene ( $\text{C}_{24}\text{H}_{12}$ ) using the PAHdb website, with the tool configured in the General options to use wavelength for the primary (bottom)  $x$ -axis.

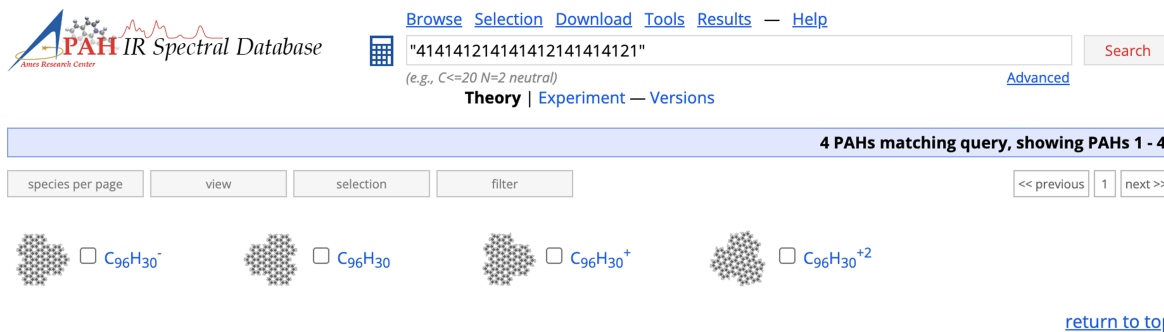


**Figure 6.** PAHdb version 4.00 search results using a boundary-edge code search string. The input code is used to perform a PAHdb search by generating a conventional PAHdb search string as determined from the code digits.

## 5. Documentation and Resources

Extensive documentation is provided for the website and software tools, including a cookbook with data analysis recipes. The PAHdb Documentation Portal is located at <https://pahdb.github.io/>, and is constantly updated following the software development on GitHub.<sup>17</sup> Documentation includes information on installation, usage, API, release history, and examples in both IDL and Python. The PAHdb cookbook includes recipes for fitting astronomical observations, either with or without utilizing the Monte Carlo approach, and using advanced emission models like considering a Kurucz stellar model.

The PAHdb website has been expanded with videos, which include tutorials, lectures, and presentations from scientific

conferences related to PAHdb analysis that are hosted on the PAHdb YouTube channel.<sup>18</sup>

## 6. Astronomical Application

The most straightforward way to demonstrate the improvements the library of computed spectra at version 4.00 brings is to compare and contrast the results of a blind database fit to those using the prior 3.20 version of the library while making use of a Monte Carlo technique to take observational uncertainties into account. Furthermore, JWST is providing unprecedented spatial-spectral observations of the IR Universe and is the benchmark to meet. Therefore, the atomic photodissociation region spectrum of the Orion Bar (R. Chown et al. 2024) from the PDRs4All program is used for assessing the impact of the new library (see R. Chown et al. 2024 for

<sup>17</sup> <https://github.com/PAHdb>

<sup>18</sup> <https://www.youtube.com/@pahdb>

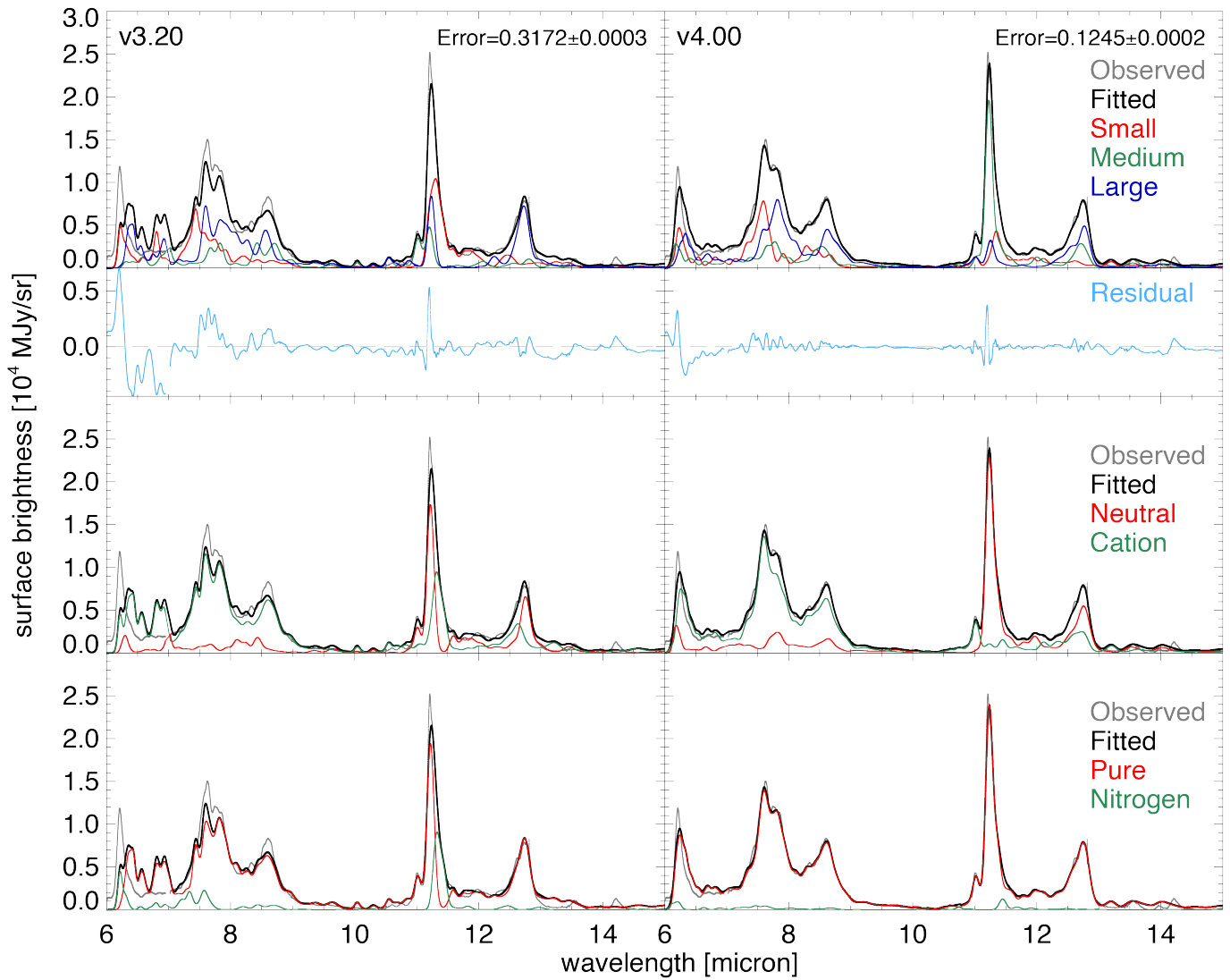


**Figure 7.** Comparison of the Monte Carlo fit to the 6–15  $\mu\text{m}$  isolated PAH component of the JWST spectrum of the atomic PDR of the Orion Bar fitted using the library of computed spectra at version 3.20 (left) and 4.00 (right). First row: observed spectrum (gray) and fit (black) broken down into contributions from small ( $20 < N_C \leq 50$ ; red), medium ( $50 < N_C \leq 70$ ; green), and large ( $N_C > 70$ ; blue) PAHs. Second row: residual. Third row: charge breakdown of the fit into contributions from PAH neutrals (red) and cations (green). Fourth row: compositional breakdown of the fit into contributions from pure PAHs (red) and nitrogenated PAHs (green). NB the observational uncertainties are less than the perceived thickness of the lines.

details on the observations and data reduction procedures of the JWST spectrum).

Figure 7 compares the results when using version 3.20 and version 4.00 of the library of DFT-computed PAH spectra. Here, emission spectra were synthesized using the parameters summarized in Table 2. Notably, this includes *not* applying a  $15\text{ cm}^{-1}$  redshift as done in a number of other studies (e.g., C. Boersma et al. 2018; A. Maragkoudakis et al. 2022), as it has been shown not to be required (C. J. Mackie et al. 2018). Furthermore, the newly added nitrogenated PAHs have been disregarded in favor of only considering those already present in version 3.20, as including them leads to an unrealistic interpretation of the results (see A. Maragkoudakis et al. 2025b). In addition, PAH anions are ignored as they are only expected to be present well below the  $10^{-2}$  level (A. G. G. M. Tielens 2005) at the Orion Bar. The AmesPAHdbIDLSuite is utilized to perform the analysis, see the Appendix, and the subclass breakdown is presented in Table 3.

**Table 2**  
Fit Model Parameters

Parameter	Value
Pool <sup>a</sup>	O = 0, Mg = 0, Fe = 0, Si = 0, CH = 0, CH <sub>2</sub> = 0, CH <sub>3</sub> = 0, CH <sub>x</sub> = 0, C > 20, H > 0, charge > -1
Model	Full emission cascade
$E_{\text{in}}$	8 eV
$\lambda_{\text{min}}$	6 $\mu\text{m}$
$\lambda_{\text{max}}$	15 $\mu\text{m}$
Line profile	Gaussian
FWHM	20 $\text{cm}^{-1}$ if $\lambda < 10\text{ }\mu\text{m}$ 15 $\text{cm}^{-1}$ if $10 \leq \lambda \leq 15\text{ }\mu\text{m}$ 10 $\text{cm}^{-1}$ if $\lambda > 15\text{ }\mu\text{m}$
$N_{\text{carbon,min}}$	21
$N_{\text{carbon,max}}$	384
Method	Monte Carlo
Samples	1024

**Note.**

<sup>a</sup> Only version 3.20 nitrogenated PAHs are considered, as well as the fullerenes, which have  $H = 0$ .



**Table 3**  
Monte Carlo PAHdb-fit Breakdown

	Charge			Size				Composition	
	Anion (%)	Neutral (%)	Cation (%)	Small (%)	Medium (%)	Large (%)	$\overline{N}_C^a$ (#)	Pure (%)	Nitrogen (%)
v3.20	...	28.19 $\pm$ 0.02	71.81 $\pm$ 0.02	37.70 $\pm$ 0.02	9.7 $\pm$ 0.1	52.6 $\pm$ 0.1	77 $\pm$ 45	86.100 $\pm$ 0.005	13.899 $\pm$ 0.005
v4.00	...	35.14 $\pm$ 0.04	64.86 $\pm$ 0.04	31.35 $\pm$ 0.05	28.3 $\pm$ 0.1	40 $\pm$ 0.1	76 $\pm$ 37	96.20 $\pm$ 0.02	3.80 $\pm$ 0.02 <sup>b</sup>

**Notes.**

<sup>a</sup> Uncertainty is the average of the standard deviations and not the standard deviation of the average number of carbon atoms.

<sup>b</sup> Only version 3.20 nitrogenated PAHs are used.

The fit shows a dramatic improvement when going from version 3.20 to version 4.00, with the average absolute error dropping from about 32% to only 12%. In terms of subclass breakdown, the delineation between size and charge becomes much more pronounced in the spectrum: the 11.2  $\mu\text{m}$  PAH band moves from a contribution of an about equal mixture of small- and large-sized PAHs to being dominated by medium-sized ones. Regarding charge, the contribution of cations to the 11.2  $\mu\text{m}$  PAH band is relegated to only the 11.0  $\mu\text{m}$  satellite feature. The need for nitrogenated PAHs drops by more than 10%. It is noted that when anions are included, their contribution drops from about 50% to 20% when moving from version 3.20 to version 4.00. Notable are the improvements in matching the 6.2  $\mu\text{m}$  PAH band and the 10–15  $\mu\text{m}$  emission (see also A. Ricca et al. 2024).

The standard deviation on the absolute errors is extremely small ( $\leq 3 \times 10^{-4}$ ), as are those given in Table 3 for the breakdown uncertainties. This is because they are derived using observational uncertainties alone, which are exceptionally small for the JWST data ( $\text{SNR}_{\text{median}} = 36$ ). Any systematic uncertainties associated with the spectra in PAHdb, which are currently unquantified, would dominate those introduced by the observations. That is, the differences between the breakdowns from version 3.20 and version 4.00 do not fall within a shared uncertainty envelope, demonstrating that they are indeed driven by the changes between both versions of the computational library. Therefore, while the absolute error and breakdown values are provided at a precision up to the first nonzero digit of the uncertainty, they are likely no more precise than up to the decimal point.

For the average number of carbon atoms ( $\overline{N}_C$ ), Table 3 reports the uncertainty of the average of the standard deviations and not the standard deviation of the average  $\overline{N}_C$ , like for the other entries. This would be taking a double average, being  $\ll 1$ . The average of the standard deviations provides an indication of how large the spread in overall PAH sizes is.

## 7. Summary and Outlook

Version 4.00 of the library of computed spectra of the PAHdb has seen a significant increase in the number of available PAH spectra. The software tools offered through PAHdb have been significantly expanded, including optimizations made to more efficiently handle the large number of spectra now available. Major improvements have been made to the PAHdb website, which now offers new libraries of laboratory and computed PAH cluster spectra. PAH boundary-edge codes are now being used throughout PAHdb to hold structural information and to search for specific PAH isomers.

All enhancements and updates are described in expanded documentation. As a demonstration, the updated version 4.00 computational library and improved software tools are used to analyze the JWST spectrum of the atomic photodissociation region of the Orion Bar and show a remarkable improvement in matching the 6.2  $\mu\text{m}$  emission band and the 10–15  $\mu\text{m}$  emission over earlier library versions.

PAHdb’s libraries will continue to expand and new libraries of PAH and PAH-related species are being prepared, including those of UV/Vis spectra of PAHs and spectra computed taking anharmonicity into account (C. J. Mackie et al. 2015, 2016, 2018, 2021, 2022; V. J. Esposito et al. 2024a, 2024b, 2024a, 2024b, 2024c). A study is underway looking into degeneracies when employing database fitting techniques (A. Maragkoudakis et al. 2025, in preparation), and implementing alternative curve-fitting approaches like Bayesian regression is under development.

## Acknowledgments

A.R., C.B., J.E.R., A.M., and L.J.A. acknowledge support from the Internal Scientist Funding Model (ISFM) Laboratory Astrophysics Directed Work Package at NASA Ames (22-A22ISFM-0009). A.R. and J.E.R. are grateful for funding through the SETI Institute cooperative agreement 80NSSC23M0046. C.B. is grateful for an appointment at NASA Ames Research Center through the San José State University Research Foundation (80NSSC22M0107). A.M. is thankful for an appointment at NASA Ames Research Center through the Bay Area Environmental Research Institute (80NSSC19M0193 and 80NSSC23M0028). M.J.S. was supported by an appointment to the NASA Postdoctoral Program at NASA Ames Research Center, administered by the Universities Space Research Association under contract with NASA. The PAHdb has been supported through a directed Work Package at NASA Ames titled: “Laboratory Astrophysics—The NASA Ames PAH IR Spectroscopic Database.”

*Facilities:* JWST.

*Software:* IDL Astronomy User’s Library (W. B. Landsman 1993), AmesPAHdbIDL Suite (The PAHdb Team 2025), AmesPAHdbPython Suite (The PAHdb Team 2022), and pyPAHdb (The PAHdb Team 2024).

## Appendix Monte Carlo Fitting Approach

The Monte Carlo fitting approach can either be configured to perturb the observations within their associated uncertainties using the default normal (Gaussian) or a uniform distribution. The number of iterations is set by default to 1024, but can be adjusted. Python and IDL codes demonstrating the use of the

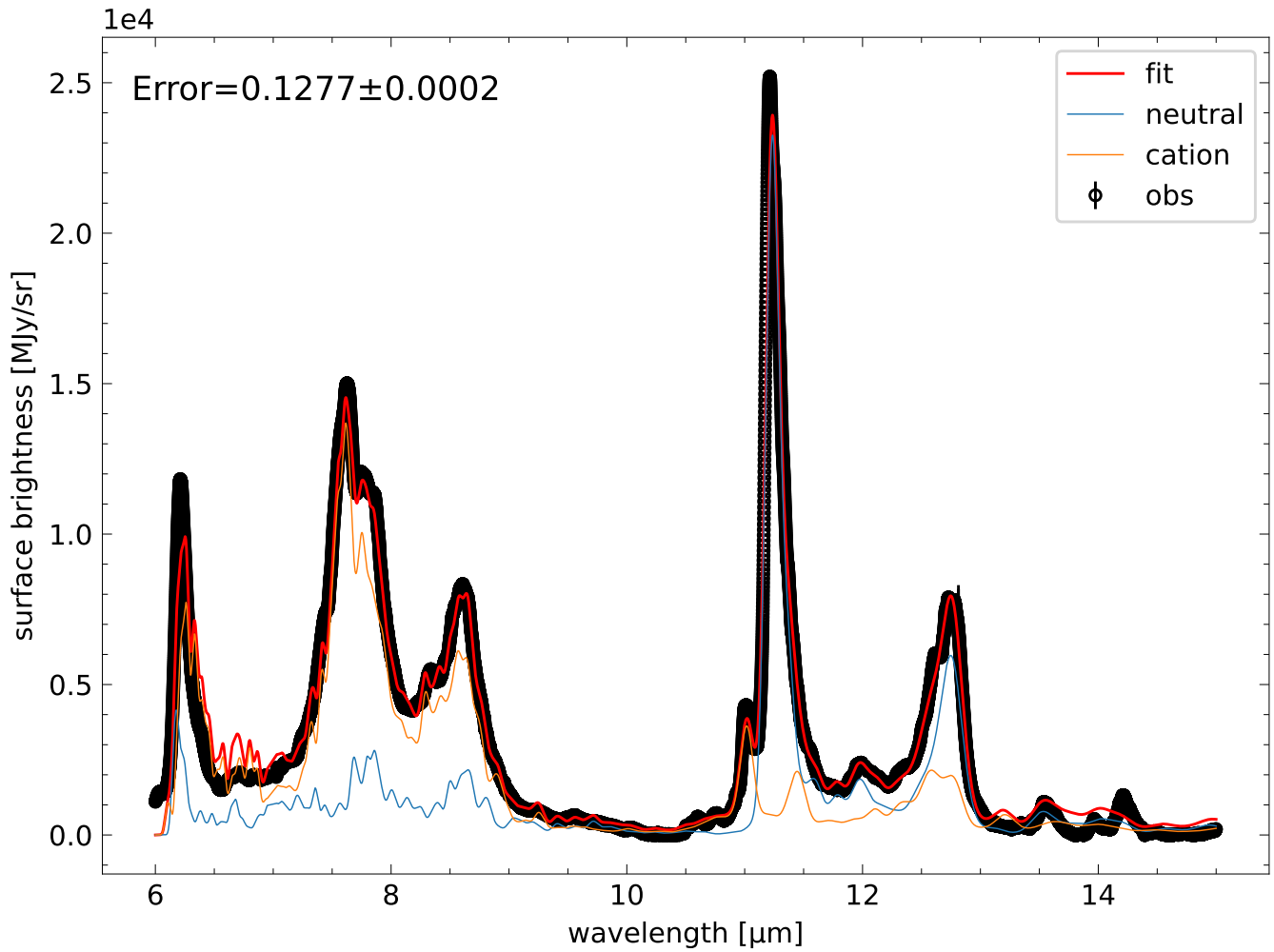


**Figure 8.** Result of a Monte Carlo fit to the 6–15  $\mu\text{m}$  isolated PAH component of the JWST spectrum of the atomic PDR of the Orion Bar fitted using the library of computed spectra at version 4.00 and the AmesPAHdbPythonSuite. The observed spectrum (open circles) is fit (red) and broken down into contributions from PAH neutrals (blue) and cations (orange). NB the uncertainties are less than the perceived thickness of the lines. The error on the fit is about  $13\% \pm 0.02\%$ .

Monte Carlo fitting approach are given in Listings 1 and 2, respectively. Figure 7 shows the result when using very similar code to the IDL case, and Figure 8 provides the result for the breakdown in terms of PAH charge when using the AmesPAHdbPythonSuite and the isolated PAH component of the JWST spectrum of the atomic PDR of the Orion Bar from Figure 7. The parameters mirror those of Table 2, except a fixed FWHM of  $10 \text{ cm}^{-1}$  is used for the line profiles. The results are comparable to those of Figure 7. The standard deviation of the error is negligible ( $2 \times 10^{-4}$ ) as the uncertainties on the spectrum are extremely small. See Section 6 for a brief discussion on the precision.

**Listing 1.** Python code snippet. Similar code can be found in “mc\_fit\_a\_spectrum.py,” located in the “examples” directory of the AmesPAHdbPythonSuite and as a recipe in the online PAHdb cookbook; [https://pahdb.github.io/cookbook/sec\\_02-mcfit\\_a\\_spectrum.html](https://pahdb.github.io/cookbook/sec_02-mcfit_a_spectrum.html).

```
from amespahdbpythonsuite.observation import Observation
from amespahdbpythonsuite.amespahdb import AmesPAHdb
```

```
# read observations into obs
obs = Observation("myFile")
```

```
# turn wavelength into frequency
```

(Continued)

```
obs.abcissaunitsto("1/cm")
```

```
# read in the database
```

```
pahdb = AmesPAHdb(filename="pahdb-complete-theoretical-v4.00.xml")
```

```
# search for the UIDs for a subset of PAHs
```

```
uids = pahdb.search("magnesium=0 oxygen=0 iron=0 silicium=0 ch=0
ch2=0 ch3=0 c>20 h>0")
```

```
# retrieve the transitions from the database for the subset of PAHs
```

```
transitions = pahdb.gettransitionsbyuid(uids)
```

```
# calculate the emission spectrum at the temperature reached
```

```
# after absorbing a 8 eV (CGS units) photon.
```

```
transitions.cascade(8 * 1.603e-12)
```

```
# convolve the bands with a Gaussian with FWHM of 15 /cm
```

```
spectrum = transitions.convolve(grid=obs.getgrid(),
```

```
  fwhm=15.0,
```

```
  Gaussian=True)
```

```
# fit the spectrum using Monte Carlo approach
```

```
mcfit = spectrum.mcfit(obs)
```

```
# plot different aspects of the fit
```

(Continued)

---

```
mcfit.plot(wavelength=True, residual=True)
mcfit.plot(wavelength=True, size=True)
mcfit.plot(wavelength=True, charge=True)
mcfit.plot(wavelength=True, composition=True)
```

---

**Listing 2.** IDL code snippet. Similar code can be found in “mc\_fit\_a\_spectrum.pro,” located in the “examples” directory of the *AmesPAHdbIDLSuite* and as a recipe in the online PAHdb cookbook; [https://pahdb.github.io/cookbook/sec\\_02-mcfit\\_a\\_spectrum.html](https://pahdb.github.io/cookbook/sec_02-mcfit_a_spectrum.html).

---

```
; read observations into AmesPAHdbIDLSuite_Observation
observation = OBJ_NEW('AmesPAHdbIDLSuite_Observation', $
    'myFile', $
    Units=AmesPAHdbIDLSuite_CREATE_OBSERVATION_UNITS_S())

; turn wavelength into frequency
observation->AbscissaUnitsTo,1

; read in the default database defined by the environment variable
; !AMESPAHDEFAULTDB or the system variable AMESPAHDEFAULTDB. use
; the keyword FILENAME if these have not been set
pahdb = OBJ_NEW('AmesPAHdbIDLSuite')

; search for the UIDs for a subset of PAHs
uids = pahdb->Search
    ('magnesium=0 oxygen=0 iron=0 silicium=0 ch=0 ch2=0 ch3=0 c>20 h>0")

; retrieve the transitions for the subset of PAHs
transitions = pahdb->getTransitionsByUID(uids)

; apply full temperature cascade emission model with an 8 eV photon
transitions->Cascade,8D*1.602D-12

; convolve the transitions into a spectrum
spectrum = transitions->Convolve(Grid=observation->getGrid(), $
    FWHM=15D, $
    /Gaussian)

; clean up transitions
OBJ_DESTROY,[transitions]






; fit the spectrum using Monte Carlo approach
mcfit = spectrum->MCFit(observation)

; plot different aspects of the fit
mcfit->Plot,/Wavelength
mcfit->Plot,/Wavelength,/Size
mcfit->Plot,/Wavelength,/Charge
mcfit->Plot,/Wavelength,/Composition

OBJ_DESTROY,[mcfit, spectrum, transitions, pahdb, observation]
```

---

## ORCID iDs

A. Ricca  <https://orcid.org/0000-0002-3141-0630>  
 C. Boersma  <https://orcid.org/0000-0002-4836-217X>  
 A. Maragkoudakis  <https://orcid.org/0000-0003-2552-3871>  
 J. E. Roser  <https://orcid.org/0000-0002-1806-3494>  
 Matthew J. Shannon  <https://orcid.org/0000-0001-5681-5151>  
 L. J. Allamandola  <https://orcid.org/0000-0002-6049-4079>  
 Charles W. Bauschlicher, Jr.  <https://orcid.org/0000-0003-2052-332X>

## References

- Andrews, H., Boersma, C., Werner, M. W., et al. 2015, *ApJ*, **807**, 99  
 Andrews, H., Candian, A., & Tielens, A. G. G. M. 2016, *A&A*, **595**, A23  
 Bakes, E. L. O., Tielens, A. G. G. M., & Bauschlicher, C. W. J. 2001a, *ApJ*, **556**, 501  
 Bakes, E. L. O., Tielens, A. G. G. M., Bauschlicher, C. W. J., Hudgins, D. M., & Allamandola, L. J. 2001b, *ApJ*, **560**, 261  
 Bauschlicher, C. W., Boersma, C., Ricca, A., et al. 2010, *ApJS*, **189**, 341  
 Bauschlicher, C. W., & Ricca, A. 2010, *MolPh*, **108**, 2647  
 Bauschlicher, C. W., Jr., Ricca, A., Boersma, C., & Allamandola, L. J. 2018, *ApJS*, **234**, 32  
 Becke, A. D. 1993, *JChPh*, **98**, 5648  
 Behlen, F. M., & Rice, S. A. 1981, *JChPh*, **75**, 5672  
 Berné, O., Habart, É., Peeters, E., et al. 2022, *PASP*, **134**, 054301  
 Bernstein, L. S., & Geballe, T. R. 2024, *ApJ*, **962**, 114  
 Boersma, C., Bauschlicher, C. W., Ricca, A., et al. 2014a, *ApJS*, **211**, 8  
 Boersma, C., Bregman, J., & Allamandola, L. J. 2018, *ApJ*, **858**, 67  
 Boersma, C., Bregman, J. D., Allamandola, L. J., Temi, P., & Maragkoudakis, A. 2024, *ApJ*, **975**, 177  
 Candian, A., Sarre, P. J., & Tielens, A. G. G. M. 2014, *ApJL*, **791**, L10  
 Cané, E., Palmieri, P., Tarroni, R., Trombetti, A., & Handy, N. C. 1996, *Gazz. Chim. Ital.*, **126**, 289  
 Castelli, F., & Kurucz, R. L. 2003, *IAUS*, **210**, A20  
 Chown, R., Sidhu, A., Peeters, E., et al. 2024, *A&A*, **685**, A75  
 Coy, B. P., Nixon, C. A., Rowe-Gurney, N., et al. 2023, *PSJ*, **4**, 114  
 Croiset, B. A., Candian, A., Berné, O., & Tielens, A. G. G. M. 2016, *A&A*, **590**, A26  
 Désesquelles, P., Ha, T. M. H., Korichi, A., et al. 2009, *JPhG*, **36**, 037001  
 Desiraju, G. R., & Gavezzotti, A. 1989a, *AcCrB*, **45**, 473  
 Desiraju, G. R., & Gavezzotti, A. 1989b, *J. Chem. Soc., Chem. Commun.*, **1989**, 621  
 Esposito, V. J., Allamandola, L. J., Boersma, C., et al. 2024a, *MolPh*, **122**, e2252936  
 Esposito, V. J., Ferrari, P., Buma, W. J., et al. 2024b, *MolPh*, **122**, e2261570  
 Esposito, V. J., Ferrari, P., Buma, W. J., et al. 2024a, *JChPh*, **160**, 114312  
 Esposito, V. J., Fortenberry, R. C., Boersma, C., & Allamandola, L. J. 2024b, *JChPh*, **160**, 211101  
 Esposito, V. J., Fortenberry, R. C., Boersma, C., Maragkoudakis, A., & Allamandola, L. J. 2024c, *MNRAS*, **531**, L87  
 Frisch, M. J., Pople, J. A., & Binkley, J. S. 1984, *JChPh*, **80**, 3265  
 Frisch, M. J., Trucks, G. W., Schlegel, H. B., et al., 2009 Gaussian 09 Revision E.01, <https://gaussian.com/g09citation/>  
 Frisch, M. J., Trucks, G. W., Schlegel, H. B., et al., 2016 Gaussian 16 Revision A.03, [https://gaussian.com/relnotes\\_a03/](https://gaussian.com/relnotes_a03/)  
 Grimme, S. 2006, *JCoCh*, **27**, 1787  
 Guo, X., Hansen, P., & Zheng, M. 2002, *Discret. Appl. Math.*, **118**, 209  
 Hansen, P., Lebatteux, C., & Zheng, M. 1996, *J. Mol. Struct. (Theochem)*, **363**, 237  
 Iyer, V. S., Wehmeier, M., Brand, J. D., Keegstra, M. A., & Müllen, K. 1997, *ACIE*, **36**, 1604  
 Kopacz, N., Corazzi, M. A., Poggiali, G., et al. 2023, *Icar*, **394**, 115437  
 Kosmaczewski, E., Stawarz, Ł., Rocha, W. R. M., Shenoy, S. S., & Karska, A. 2022, *ApJ*, **934**, 94  
 Kovács, P., Zhu, X., Carrete, J., Madsen, G. K. H., & Wang, Z. 2020, *ApJ*, **902**, 100  
 Kovič, J. 2014, *MATCH Commun. Math. Comput. Chem.*, **72**, 27  
 Landsman, W. B. 1993, *ASPC*, **52**, 246  
 López-Puertas, M., Dinelli, B. M., Adriani, A., et al. 2013, *ApJ*, **770**, 132  
 Mackie, C. J., Candian, A., Huang, X., et al. 2015, *JChPh*, **143**, 224314  
 Mackie, C. J., Candian, A., Huang, X., et al. 2016, *JChPh*, **145**, 084313  
 Mackie, C. J., Candian, A., Lee, T. J., & Tielens, A. G. G. M. 2021, *ThChA*, **140**, 124  
 Mackie, C. J., Candian, A., Lee, T. J., & Tielens, A. G. G. M. 2022, *JPCA*, **126**, 3198  
 Mackie, C. J., Chen, T., Candian, A., Lee, T. J., & Tielens, A. G. G. M. 2018, *JChPh*, **149**, 134302  
 Maragkoudakis, A., Boersma, C., Peeters, E., et al. 2025a, *ApJ*, submitted  
 Maragkoudakis, A., Boersma, C., Temi, P., Bregman, J. D., & Allamandola, L. J. 2022, *ApJ*, **931**, 38  
 Maragkoudakis, A., Boersma, C., Temi, P., et al. 2025b, *ApJ*, **979**, 90  
 Maragkoudakis, A., Peeters, E., & Ricca, A. 2020, *MNRAS*, **494**, 642  
 Maragkoudakis, A., Peeters, E., & Ricca, A. 2023a, *MNRAS*, **520**, 5354

- Maragkoudakis, A., Peeters, E., Ricca, A., & Boersma, C. 2023b, *MNRAS*, **524**, 3429
- Martins-Franco, Y., & Menéndez-Delmestre, K. 2021, *AN*, **342**, 186
- Mathis, J. S., Mezger, P. G., & Panagia, N. 1983, *A&A*, **128**, 212
- Mattioda, A. L., Hudgins, D. M., Boersma, C., et al. 2020, *ApJS*, **251**, 22
- Pasquini, S., Peeters, E., Schefter, B., et al. 2024, *A&A*, **685**, A77
- Pence, W. D., Chiappetti, L., Page, C. G., Shaw, R. A., & Stobie, E. 2010, *A&A*, **524**, A42
- Pilleri, P., Montillaud, J., Berné, O., & Joblin, C. 2012, *A&A*, **542**, A69
- Pirali, O., Vervloet, M., Mulas, G., Mallocci, G., & Joblin, C. 2009, *PCCP*, **11**, 3443
- Rapacioli, M., Calvo, F., Spiegelman, F., Joblin, C., & Wales, D. 2005a, *JPCA*, **109**, 2487
- Rapacioli, M., Joblin, C., & Boissel, P. 2005b, *A&A*, **429**, 193
- Ricca, A., Bauschlicher, C. W., & Allamandola, L. J. 2013, *ApJ*, **776**, 31
- Ricca, A., Bauschlicher, C. W. J., Roser, J. E., & Peeters, E. 2018, *ApJ*, **854**, 115
- Ricca, A., Boersma, C., & Peeters, E. 2021, *ApJ*, **923**, 202
- Ricca, A., Roser, J. E., Boersma, C., Peeters, E., & Maragkoudakis, A. 2024, *ApJ*, **968**, 128
- Ricca, A., Roser, J. E., Peeters, E., & Boersma, C. 2019, *ApJ*, **882**, 56
- Rosenberg, M. J. F., Berné, O., & Boersma, C. 2014, *A&A*, **566**, L4
- Rosenberg, M. J. F., Berné, O., Boersma, C., Allamandola, L. J., & Tielens, A. G. G. M. 2011, *A&A*, **532**, A128
- Roser, J. E., & Allamandola, L. J. 2010, *ApJ*, **722**, 1932
- Roser, J. E., & Ricca, A. 2015, *ApJ*, **801**, 108
- Roser, J. E., & Ricca, A. 2020, *IAUS*, **15**, 415
- Roser, J. E., Ricca, A., & Allamandola, L. J. 2014, *ApJ*, **783**, 97
- Sander, L. C., & Wise, S. A. 2020, NIST Special Publication 922, Polycyclic Aromatic Hydrocarbon Structure Index, NIST [https://www.NIST.gov/system/files/documents/2020/08/03/sp922\\_2020.pdf](https://www.NIST.gov/system/files/documents/2020/08/03/sp922_2020.pdf)
- Shannon, M. J., & Boersma, C. 2018, Proc. of the 17th Python in Science Conf. (SciPy), **99**
- Shannon, M. J., & Boersma, C. 2019, *ApJ*, **871**, 214
- Sidhu, A., Tielens, A. G. G. M., Peeters, E., & Cami, J. 2022, *MNRAS*, **514**, 342
- Silva-Ribeiro, A., Krabbe, A. C., Canelo, C. M., et al. 2022, *MNRAS*, **509**, 327
- Stephens, P. J., Devlin, F. J., Chabalowski, C. F., & Frisch, M. J. 1994, *JPhCh*, **98**, 11623
- The PAHdb Team, 2022 AmesPAHdbPythonSuite, v0.5.0, Zenodo, doi:[10.5281/zenodo.17428588](https://doi.org/10.5281/zenodo.17428588)
- The PAHdb Team, 2024 pyPAHdb, v1.0, Zenodo, doi:[10.5281/zenodo.17428405](https://doi.org/10.5281/zenodo.17428405)
- The PAHdb Team, 2025 AmesPAHdbIDLSuite, v3.1, Zenodo, doi:[10.5281/zenodo.17428247](https://doi.org/10.5281/zenodo.17428247)
- Tielens, A. G. G. M. 2005, The Physics and Chemistry of the Interstellar Medium (Cambridge Univ. Press)
- Tielens, A. G. G. M. 2008, *ARA&A*, **46**, 289
- Zang, R. X., Peeters, E., & Boersma, C. 2019, *ApJ*, **887**, 46